Soft Matter

Quantitative analysis of bending hysteresis by real-time monitoring of curvature in flexible polymeric films

Journal:	*Soft Matter*
Manuscript ID	SM-ART-12-2020-002233.R2
Article Type:	Paper
Date Submitted by the Author:	17-Mar-2021
Complete List of Authors:	Taguchi, Ryo; Tokyo Institute of Technology, Laboratory for Chemistry and Life Science; Tokyo Institute of Technology, Department of Chemical Science and Engineering Kuwahara, Kohei; Tokyo Institute of Technology, Laboratory for Chemistry and Life Science; Tokyo Institute of Technology, Department of Chemical Science and Engineering Akamatsu, Norihisa; Tokyo Institute of Technology, Laboratory for Chemistry and Life Science; Tokyo Institute of Technology, Department of Chemical Science and Engineering Shishido, Atsushi; Tokyo Institute of Technology, Laboratory for Chemistry and Life Science; Tokyo Institute of Technology, Department of Chemical Science and Engineering

ARTICLE

Quantitative analysis of bending hysteresis by real-time monitoring of curvature in flexible polymeric films

Received 00th January 20xx,
Accepted 00th January 20xx

DOI: 10.1039/x0xx00000x

Ryo Taguchi,[ab] Kohei Kuwahara,[ab] Norihisa Akamatsu[ab] and Atsushi Shishido*[ab]

Flexibility, viscoelasticity and stress-strain relation in bending polymeric films are key factors in designing mechanically durable flexible electronic devices and soft robots. However, bending hysteresis, which appears as a precursor phenomenon of fracture and fatigue, remains unclear; no one quantitatively evaluated a bending curvature causing hysteresis. Herein, we report the bending hysteresis of polymeric films used as common substrates in flexible electronics through precisely monitoring bending curvatures. By real-time measuring curvatures of films upon bending and subsequent unbending, we have successfully determined the curvatures that cause the hysteresis. These curvatures also depend on a film thickness. Furthermore, we revealed that the occurrence of bending hysteresis is explained by bending strains that have a nonlinear relation with internal stresses. This enables us to predict strain limits that cause the bending hysteresis, based on a stress-strain curve of polymeric films.

Introduction

Since the first studies on all polymer electronic devices have been reported in 1990s,[1–4] flexible electronic devices and soft robots are emerging and even now garnering attention in commercial and consumer good applications. Reflecting the increasing trend on flexible electronics and soft robotics, various types of flexible materials and devices have been developed, *e.g.* flexible thin-film transistors (TFTs),[5,6] flexible photovoltaic cells,[7] flexible organic light-emitting diodes (OLEDs),[8,9] flexible batteries,[10] flexible tactile pressure, strain, temperature sensors[11–13] and actuators.[14–17] The flexible electronic devices demand high performance comparable to conventional hard electronic devices.[18–21] Therefore, most flexible electronic devices recently reported employ hybrid systems that integrate mechanically flexible polymeric film substrates and inorganic materials which exhibit excellent electrical properties.

Polymer film substrates that have both high Young modulus (= 1–9 GPa) and high bendability are suitable in these systems.[18,22] In general, they exhibit bending hysteresis. For example, a polyethylene naphthalate (PEN) film, which is used as a common substrate in flexible electronic devices, does not immediately recover to the initial flat state after it undergoes a large bending with a small curvature radius (Fig. 1a-c). Such bending hysteresis causes fractures such as crack, slip and delamination at the interface between polymeric film substrates and inorganic materials, which is the present concern in the hybrid system design.[18,19,23–25] Researchers and engineers should place importance on appropriate selection of substrates based on their mechanical hysteresis properties. However, hysteresis behaviours of polymeric materials have been studied mainly on tensile deformations.[26–33] Surprisingly, the studies on bending-induced hysteresis have rarely been reported: although it is recognised that polymeric films do not exhibit hysteresis after they undergo a small bending with a large curvature radius (Fig. 1d-f), no one even evaluated the cur-

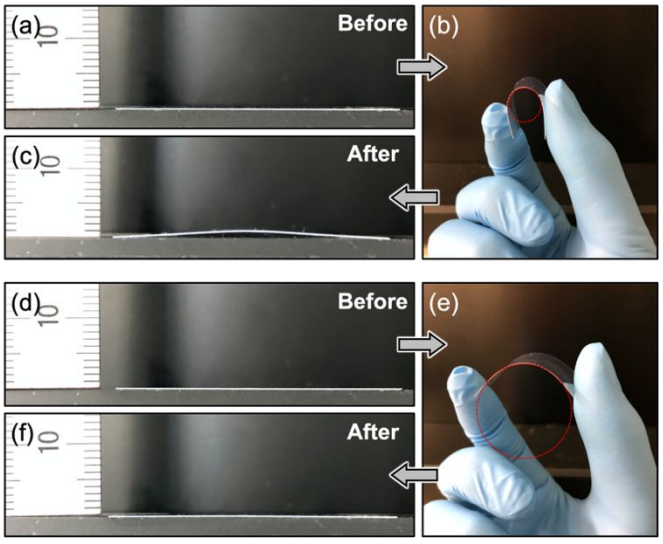

Fig. 1. Photographs of bent and unbent PEN films. The film (a) before, (b) during and (c) after large bending with a small curvature radius (red circle). The film (d) before (e) during and (f) after small bending with a large curvature radius (red circle).

[a] *Laboratory for Chemistry and Life Science, Institute of Innovative Research, Tokyo Institute of Technology, 4259 Nagatsuta, Midori-ku, Yokohama 226-8503, Japan. Email: ashishid@res.titech.ac.jp; Tel: +81-45-924-5242*
[b] *Department of Chemical Science and Engineering, School of Materials and Chemical Technology, Tokyo Institute of Technology, Ookayama, Meguro-ku, Tokyo 152-8552, Japan.*
†Electronic Supplementary Information (ESI) available: The ESI includes Fig. S1–S3. See DOI: 10.1039/x0xx00000x

vature radius threshold that begins to exhibit bending hysteresis (Fig. 1).

Recently, we have reported that bent shapes of polymeric films depend on their inherent relations between stress and strain of the materials.[34–39] This achievement has been obtained through measuring a curvature of bending polymeric films with our laboratory-made equipment.[37,39] In this article, we have evaluated bending hysteresis of PEN films by quantitatively measuring their bending curvature. This quantification successfully revealed that the film bent above a certain curvature exhibits bending hysteresis. The curvature, at which bending hysteresis occurs, also depended on a film thickness, and these dependences were well explained by bending strains calculated from thicknesses and curvatures. Through the theoretical calculations, we have revealed that bending hysteresis of the film occurs when its relations between stress and strain make the transition from linear to nonlinear. This finding enables us to predict a curvature at which hysteresis begins to occur based on calculations using stress-strain curves.

Results and discussion

To quantitatively investigate bending hysteresis behaviours that the PEN film exhibited, we captured cross-sectional images of the bending film with our laboratory-made equipment (Fig. 2a). The flat film with a length of L was bent by pushing its both edges with the distance of ΔL to the applied strain ($\Delta L/L$) of 90% (Fig. 2b), and subsequently returned to the initial state (the applied strain of 0%) (Fig. 2c). In bending and unbending processes, the captured images of bent shapes were clearly different: the shapes at the centre of the film became sharper in the unbending process than those in the bending process even at the same applied strain. Figure 2d and 2e show the curvature radius and curvature geometrically calculated from the images as a function of applied strain, respectively. In bending, the curvature radius decreased (Fig. 2d) and the curvature increased (Fig. 2e) as the applied strain increased from 0% to 90%; subsequently, the unbending, induced by decreasing the applied strain from 90% to 0%, resulted in the increase in curvature radius (Fig. 2d) and the decrease in curvature (Fig. 2e). The residual curvature disappeared after a while. This means that the PEN film behaves elastically up to the bending with the applied strain of 90%.

The degree of the bending hysteresis strongly depended on a turnaround applied strain. Figure 3a-d shows the curvatures of the 125-µm-thick PEN film in the bending and unbending processes at the turnaround applied strain of 85%, 80%, 75% and 70%. Although curvatures in the unbending process were not identical to those in the bending process at the turnaround applied strains of 85%, 80% and 75%, their hysteresis became smaller with decreasing the turnaround applied strain. It should be noted that the bending and unbending at the turnaround applied strain of 70% did not show the apparent hysteresis. Therefore, the bending hysteresis of the PEN film begins to appear at the bending where the applied strain ranges from 70% to 75%, and the degree of hysteresis expands with increas-

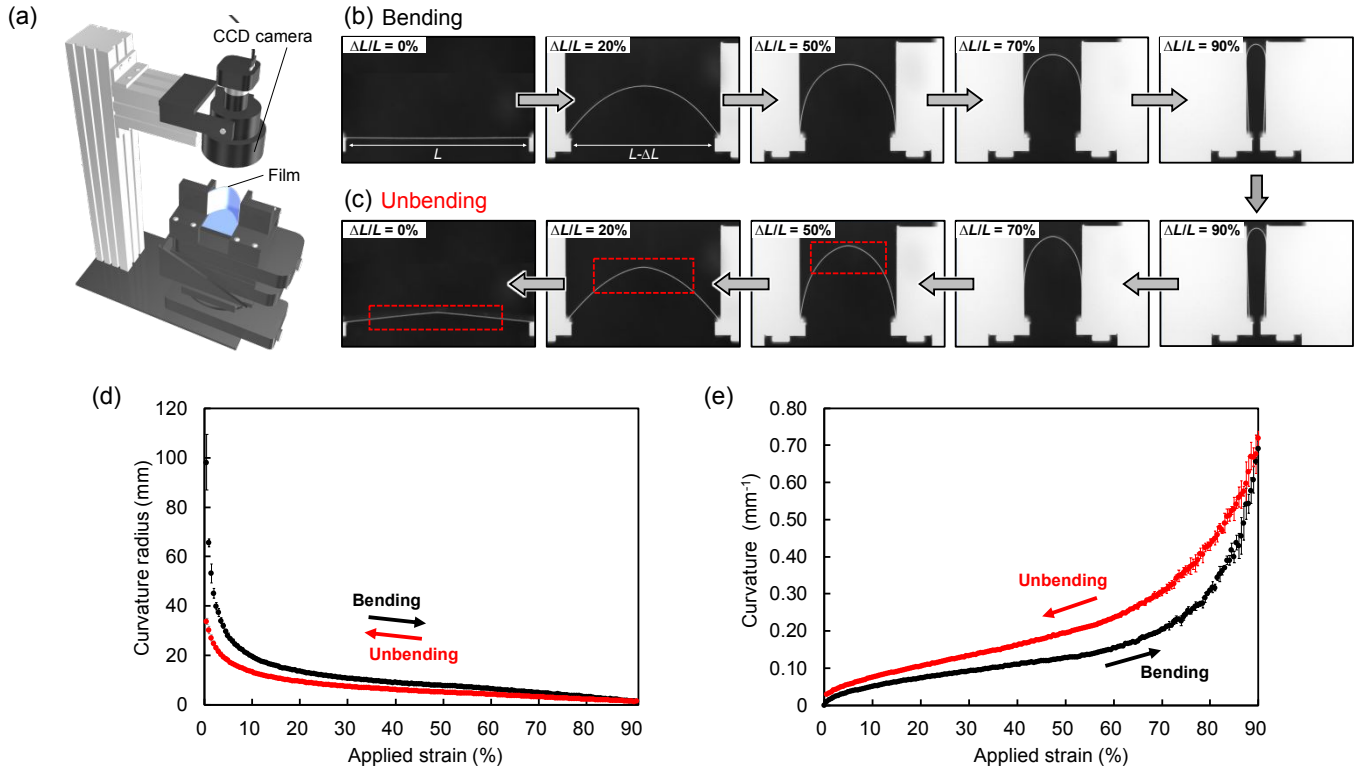

Fig. 2. (a) Illustration of the laboratory-made equipment used for measurement of curvature radius of bending films. A charge-coupled device (CCD) camera equipped captures the shape of bent films. Photographs of the PEN film during (b) bending and (c) unbending. (d) Curvature radius and (e) curvature of the PEN film with a thickness of 125 µm during bending (black plots) and subsequent unbending (red plots).

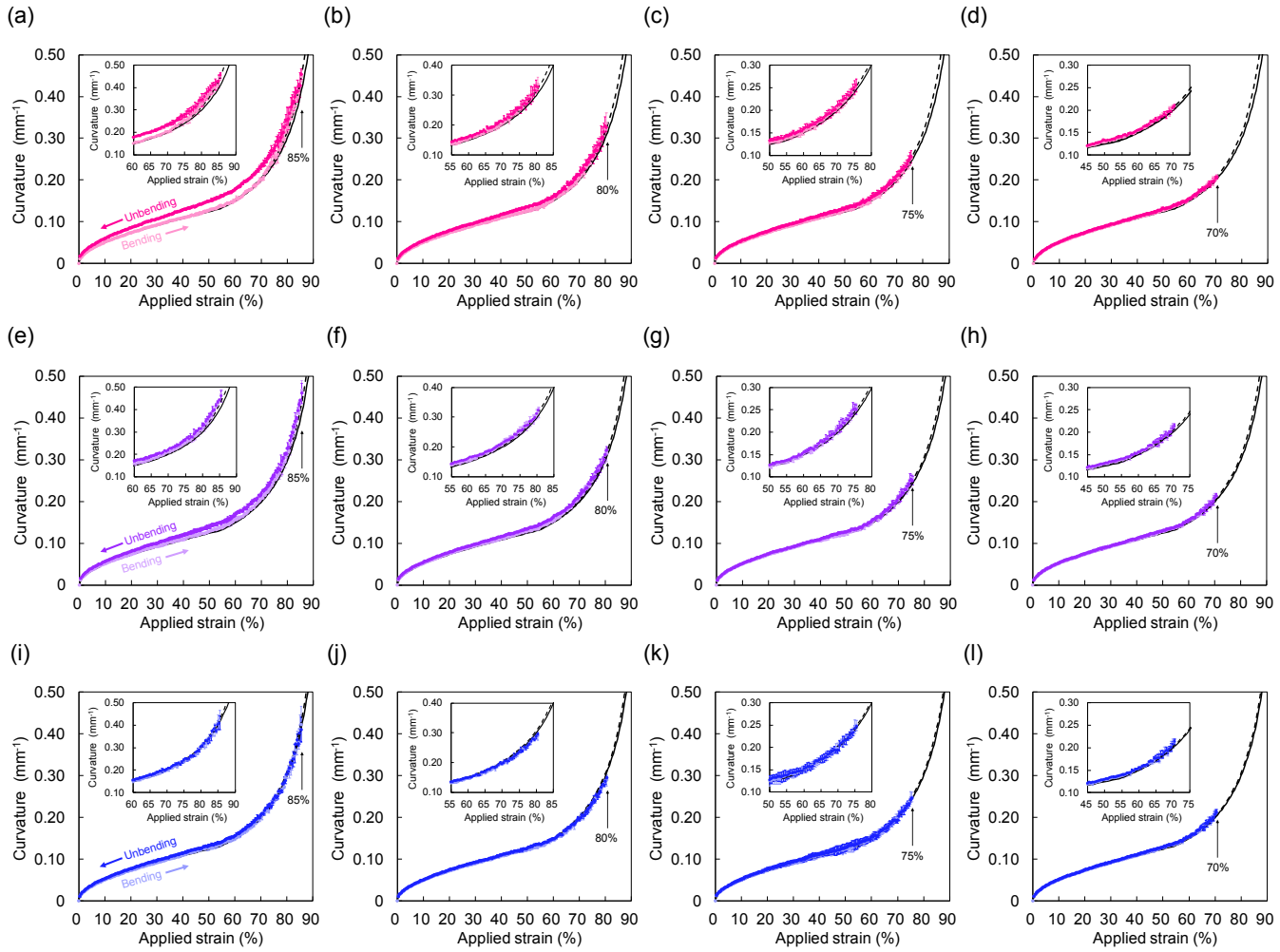

Fig. 3. Curvatures of the PEN film with a thickness of 125 μm during bending and subsequent unbending at the turnaround applied strain of (a) 85%, (b) 80%, (c) 75% and (d) 70%. Curvatures of the PEN film with a thickness of 100 μm during bending and subsequent unbending at the turnaround applied strain of (e) 85%, (f) 80%, (g) 75% and (h) 70%. Curvatures of the PEN film with a thickness of 75 μm during bending and subsequent unbending at the turnaround applied strain of (i) 85%, (j) 80%, (k) 75% and (l) 70%. Light and dark plots correspond to bending and unbending, respectively. Solid and dashed lines show the theoretical curvatures calculated from the Elastica and the modified Elastica theories, respectively. Insets show magnified graphs.

ing the turnaround applied strain.

The applied strain, at which the bending hysteresis begins to occur, depends on a thickness of the PEN film. In the case of the 100-μm-thick PEN film, the bending and unbending at the turnaround applied strains of 85% and 80% produced the bending hysteresis (Fig. 3e and 3f); however, the degrees of the hysteresis were smaller compared with those of the 125-μm-thick film. The hysteresis was not observed in bending and unbending at the turnaround applied strain below 75% (Fig. 3g and 3h), indicating that the bending hysteresis begins to appear at the bending of the applied strain between 75% and 80% for the 100-μm-thick PEN film. The thinner PEN film with a thickness of 75 μm showed the similar experimental trend: the degrees of bending hysteresis became smaller compared those for the PEN films with thicknesses of 100 and 125 μm (Fig. 3i-l); furthermore, the occurrence of bending hysteresis was suppressed in the turnaround applied strain between 80% and 85% for the 75-μm-thick film.

Of interest, the degree of hysteresis is determined by bending strains calculated from a film thickness and a curvature. The degree of hysteresis observed in bending and unbending is quantified as bending hysteresis ratio by using eqn (1):

$$Bending\ hysteresis\ ratio\ (\%) = \frac{(A_{unbending} - A_{bending})}{A_{bending}} \quad (1)$$

where A_{bending} and $A_{\text{unbending}}$ represent the areas of curvature-applied strain curves in bending and unbending processes, respectively. Figure 4a displays the bending hysteresis ratios for each case of the films tested. The bending hysteresis ratio monotonically increased with increases in a turnaround applied strain and a film thickness. Since the bending strains (ε) in a film are the product of the distance from the middle of thickness (z) and the curvature ($1/R$: R is the curvature radius at the film cent-

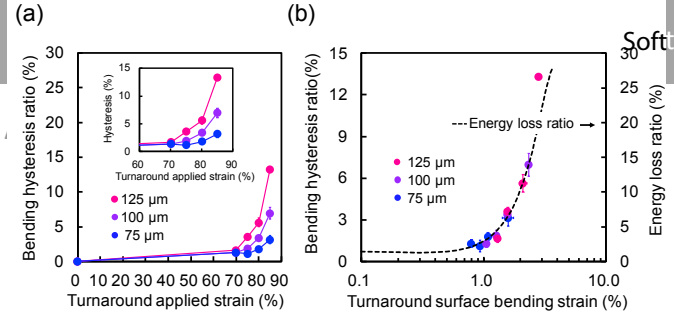

Fig. 4. Bending hysteresis ratio for the PEN films with thicknesses of 125 μm (pink plots), 100 μm (purple plots) and 75 μm (blue plots) as a function of (a) turnaround applied strain and (b) turnaround surface bending strain. A dashed line shows the energy loss ratio calculated from internal stresses.

re), they can be calculated from $\varepsilon = z/R$. For example, the surface bending strain can be calculated from $h/2R$ (where h represents a film thickness). We have found that the increase in the bending hysteresis ratio of each film shows a similar trend for the turnaround surface bending strain (Fig. 4b). This result indicates that the increase in bending strain imposed on the films lead to the extensive bending hysteresis.

The large bending strain within a nonlinear region in a stress-strain (S-S) curve induces the bending hysteresis. Figure 5 shows the S-S curve of a PEN film, which was obtained at the strain rate of 0.3% min^{-1} similar to the bending strain rate. The strain range of the S-S curve that follows Hooke's law is in the linear-elastic region, which corresponds to approximately <1.1% strains; the other range shows the nonlinear-elastic region (or the plastic region), which corresponds to approximately >1.1% strains. By imposing the tensile strain within the linear-elastic range (0.5%) upon the PEN film and subsequently removing it, the loading and unloading curves became identical. In contrast, the unloading stress was lowered when the tensile strains within the nonlinear-elastic range (1.5% and 3.0%) was applied to the PEN film and then removed. This energy loss is generally observed by applying large strains

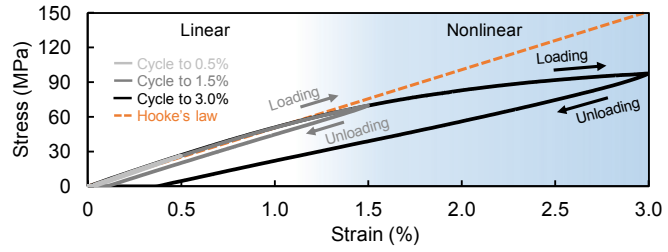

within nonlinear region of S-S curves as can be seen in Fig. S1. Similar to such tensile deformation, the nonlinear-elastic bending, whose bending strains are within the nonlinear region

Fig. 5. Stress-strain curve of the PEN film. The cycle curves of uniaxial mechanical testing to 0.5%, 1.5% and 3.0% strains. White and blue areas correspond to the linear and the nonlinear regions, respectively. The dashed line shows Hooke's law.

of the S-S curve, may lower the internal stress in unbending process due to the energy loss. Here, we assume that S-S curves of the film upon tension and compression are equivalent, and thereby, can calculate the stress (σ) from the S-S curve formulated by the following equation: [37,39]

$$\sigma = \sum_{i=1}^{n} \mathrm{sgn}(\varepsilon^{i-1}) E_i \varepsilon^i \qquad (2)$$

where E_i represent the polynomial coefficient, and the higher polynomial degree can accurately fit the curve. By approximating the loading curve with the polynomial function of degree six (n = 6), we determined E_i as shown in Fig. S2a. Unlike the tensile deformation where the internal stress at the vertical cross-section to the mechanical direction is uniform, the internal stresses of a bent film have the gradient in the thickness direction. They can be calculated via bending strain ($\varepsilon = z/R$) in the film that fulfils the Bernoulli-Euler beam condition in which the vertical cross-section is perpendicular to the material axis under bending (Fig. 6a).[40] Thus, eqn (2) can be rewritten as:

$$\sigma_{bending} = \sum_{i=1}^{n} \mathrm{sgn}\left[\left(\frac{z}{R}\right)^{i-1}\right] E_i \left(\frac{z}{R}\right)^i. \qquad (3)$$

By calculating eqn (3), we obtained the internal stress distribution at the central cross-section of the 125-μm-thick PEN film bent with the applied strain of 55% ($1/R$ = 0.137 mm^{-1}) as a typical example (Fig. 6b). Figure 6c shows internal stress distributions in bending process at various applied strains. We have found that the bending with applied strain of >75% becomes nonlinear-elastic. Next, let us consider the internal stress distribution in unbending process. Supposing that the relation between stress and strain is linear upon unloading, the unloading S-S curve is $\sigma = A\varepsilon + B$. The slope ($A$) and the intercept ($B$) depend on the turnaround strain (ε_{ta}) as shown in Fig. S2b; thus, A and B can be expressed as polynomial functions of $\sum_{i=1}^{m} A_i {\varepsilon_{ta}}^i$ and $\sum_{i=1}^{n} B_i {\varepsilon_{ta}}^i$ where A_i and B_i represent the polynomial coefficient obtained by approximating the slope and intercept curves in Fig. S2b with the polynomial function, respectively. We assume the equivalent S-S curves in tension and compression again, and the internal stress in the unbending process is given as a function of turnaround strain ($\varepsilon_{ta} = z/R_{ta}$ where R_{ta} represents the turnaround curvature radius):

$$\sigma_{unbending} = \sum_{i=1}^{m} \mathrm{sgn}\left[\left(\frac{z}{R_{ta}}\right)^i\right] A_i \left(\frac{z}{R_{ta}}\right)^i \left(\frac{z}{R}\right) + \sum_{i=1}^{l} \mathrm{sgn}\left[\left(\frac{z}{R_{ta}}\right)^{i-1}\right] B_i \left(\frac{z}{R_{ta}}\right)^i. \qquad (4)$$

The least squares method determined A_i (m = 4) and B (l = 3), and then, the calculations of eqn (4) yielded the internal stress distributions upon unbending (Fig. 6d). We found that the internal stresses in unbending process decreases as the turnaround applied strain increases. These decreases occur after the nonlinear elastic bending as shown in Fig. 6b-d. Similar trends were also observed from the calculations of internal stre-

Fig. 6. (a) A model of the bending film at the applied strain of 55%. The bent film is assumed to have vertical cross-section perpendicular to the material axis as shown in the magnified illustration. (b) Internal stress distribution of the PEN film upon bending with the applied strain of 55%.

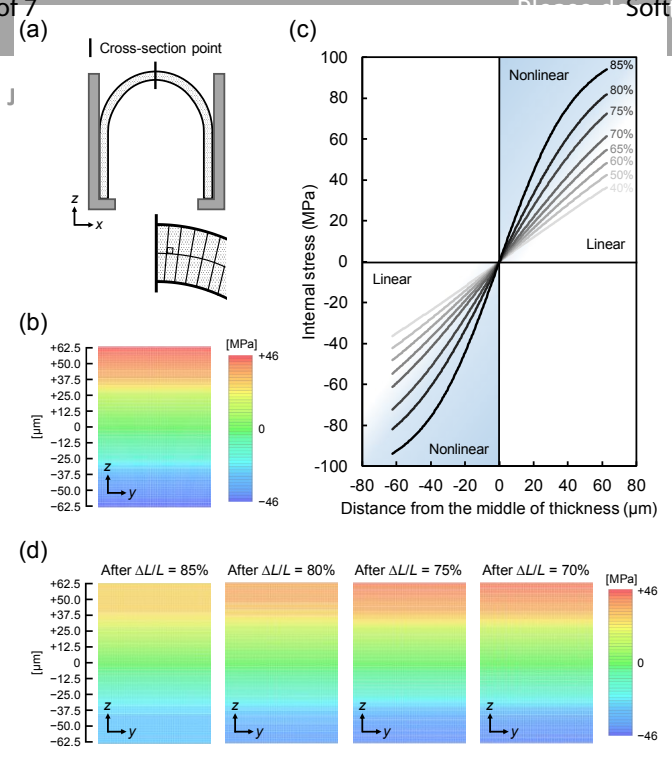

(c) Internal stresses in the thickness direction of the PEN film bent with various applied strains. (d) Internal stress distribution of the PEN film bent with the applied strain of 55% in unbending process at turnaround applied strains of 85%, 80%, 75% and 70%.

ss distributions for the films with thicknesses of 100 μm and 75 μm (Fig. S3). The internal stresses obtained in bending and unbending processes were converted to an energy loss ratio using the following equation:

$$Energy\ loss\ ratio\ (\%) = \frac{\int_0^{\frac{h}{2}}\int_0^{\rho_{ta}}(\sigma_{bending} - \sigma_{unbending})d\rho dz}{\int_0^{\frac{h}{2}}\int_0^{\rho_{ta}}\sigma_{bending}d\rho dz} \quad \#(5)$$

where ρ (=1/R) is curvature, and namely, $\rho_{ta} = 1/R_{ta}$. The energy loss ratio as a function of turnaround surface bending strain agreed with the bending hysteresis (see the dashed line in Fig. 4b). This result indicates that the energy loss caused by the nonlinear-elastic bending results in the bending hysteresis, suggesting that the observed bending hysteresis has the origin similar to a typical tensile deformation as follows: large strain within the nonlinear-elastic region, imposed on the outer surface of the film, elongate polymer main chains along the tensile direction and thereby generates the friction heat dissipation due to slipping of the polymer main chains. This energy loss in the nonlinear-elastic bending causes the curvature difference in the bending and unbending processes.

On the basis of the above understanding, we can predict the bending parameters that cause the bending hysteresis, such as the applied strain, the film thickness and the curvature radius. Recently, we have established the modified Elastica theory which provides numerical solutions of curvature radius of bending polymeric films.[37,39] The film shapes in the nonlinear-elastic bending exhibit the smaller curvature radius (*i.e.*, the larger curvature) compared to those in the linear-elastic bending at the same applied strain, which can be calculated from S-S curves of polymeric films. Since a curvature radius in the linear-elastic bending is in accordance with that of the classic beam theory,[37,39,40] bending behaviour with no bending hysteresis follows the Elastica theory (see solid lines in Fig. 3d, 3g, 3h, 3j, 3k and 3l). In contrast, the modified Elastica theory agreed with the bending curvatures exhibiting the hysteresis in unbending (see dashed lines in Fig. 3a, 3b, 3c, 3e, 3f and 3i). These results also support that the nonlinear-elastic bending leads to the bending hysteresis, indicating that we can predict the turnaround curvatures at which the bending hysteresis begins based on the Elastica and modified Elastica theories. The theories will help the design of polymeric films for developing mechanically durable flexible electronic devices. Note that the theories are applicable only to the small strain range where tensile and compressive S-S curves are equivalent.[37,39–41] For example, polymer films, of which one surface undergoes plastic deformation, are beyond the applicable limits of the theories. The detailed calculation procedure of the theories is shown in Experimental section.

Experimental

Film samples.

PEN films (Q65-HA) with thicknesses of 125 μm, 100 μm and 75 μm were purchased from Teijin Limited. The films were cut to the sizes of 30 (height) × 40 (width) mm^2 for bending curvature measurements.

Real-time measurement of curvature upon bending and unbending.

Films were bent at the applied strain rate of 8.5% min^{-1}. The curvature of bent films was measured using the image analysis technique previously reported.[37,39] First, images of the bent films were captured in real time using a CCD camera. Subsequently, the shape profiles of the films were fitted using a sixth-order function. Finally, the curvature was geometrically calculated from the obtained function. Unless otherwise stated, all measurements were taken at least thrice for each film. In addition, for each film type, three samples were measured. Curvature values and error bars in figures represent the means and standard deviations of the respective measurement results.

Mechanical tensile tests.

All mechanical tensile tests were performed on an INSTRON 5943 at a strain rate of 0.3% min^{-1}. The strain rate was set to match the bending strain rate (= average 0.29% min^{-1}). Each film cut to the sizes of a gauge length of 100 mm and a wide of 5 mm was loaded up to an arbitrary turnaround tensile strain, and then, the load was removed.

Calculations of internal stress distributions upon bending and unbending.

1) Internal stress upon bending. We approximated the measured S-S curves by the least squares method of the polynomial degree of six (Fig. S2a), and then obtained each eqn (2) and (3). Using eqn (3), the internal stresses in the thickness direction

were calculated for films bent with each applied strain. The internal stress distribution of the film bent with the applied strain of 55% was also calculated from eqn (3). The number of square elements with a dimension of 0.5 μm is approximately 45,000.

2) Internal stress upon unbending. We approximated the slope and intercept of unloading S-S curves as a function of turnaround strain by the least squares method of the polynomial degree of four and three, respectively (Fig. 2b). As a result, we obtained eqn (4). The calculation of eqn (4) yields the internal stress distributions of the film bent with the applied strain of 55% after bending to an arbitrary turnaround applied strain.

Calculations of the Elastica theory and the modified Elastica theory.

1) The Elastica theory.[37,39,40] A film was modelled as a beam of a linear-elastic material with length (L), width (w) and thickness (h). An axial compression to the film edges bends the film with an angle of the film edge (θ). The angle θ allows for the analysis of the curvature ($1/R$) and the applied strain ($\Delta L/L$) in the range of $0 \le \theta \le \pi/2$, as follows:

$$\frac{1}{R} = \frac{4pK(p)}{L} \tag{6}$$

$$\frac{\Delta L}{L} = 2\left[1 - \frac{E(p)}{K(p)}\right] \tag{7}$$

where $K(p)$ and $E(p)$ denote the complete elliptic integrals of the first and second kind, respectively. The symbol p denotes $\sin(\theta/2)$. For $\theta = \pi/2$, the curvature ($1/R$) is calculated as a function of ΔL from the equation:

$$\frac{1}{R} = \frac{2\sqrt{2}[2E(p) - K(p)]}{L} \tag{8}$$

By using eqn (6)–(8), the theoretical curvature was calculated in MATLAB.

2) The modified Elastica theory.[37,39] A film was modelled as a beam of length (L), width (w) and thickness (h) again. Let s be the distance along the axis of the bent film from origin O; the expression for the angle between the line tangent to the bent film and the x-axis is $\vartheta(s)$ (*the angle $\vartheta(0)$ corresponds to the angle θ). The S-S curve of the PEN film were also expressed as eqn (2). The value of $[d\varphi(s)/ds]_{s=L/2}$ where $\varphi(s)$ denotes $\arcsin[(\vartheta(s)/2)/\sin(\theta/2)]$ was calculated from eqn (2), then giving numerical solutions of curvatures at each applied strain using the two equations below:

$$\frac{1}{R} = -2\sin\frac{\beta}{2}\left[\frac{d\varphi(s)}{ds}\right] \tag{9}$$

$$\frac{\Delta L}{L} = 1 - \frac{\int_o^L \left(\frac{dx}{ds}\right) ds}{L} \tag{10}$$

All calculations were performed using MATLAB. The detailed calculations are described in our previous report.[37,39]

Conclusions

We have evaluated bent shapes of PEN films during bending and subsequent unbending through real-time measurements of curvatures. The films, bent above a certain curvature, exhibited hysteresis during unbending. The increase in a turnaround curvature results in larger hysteresis. The degree of hysteresis also depends on the thickness of films. The theoretical calculation shows that bending strains in a nonlinear region in terms of stress cause hysteresis in the unbending process. These findings successfully enable us to predict strain limit of reversible bending in various films by combining a S-S curve with the Elastica and modified Elastica theories. Such predictions could be useful in designing polymeric film substrates integrated into flexible electronics, preventing the failure of the devices.

Conflicts of interest

There are no conflicts to declare.

Acknowledgements

This work was supported by a Grant-in Aid for Scientific Research on Innovative Areas “Molecular Engine” (JSPS KAKENHI Grant Number JP18H05422). This work was supported by JSPS KAKENHI Grant Number JP20K15339. This work was supported by JST CREST Grant Number JPMJCR18I4, Japan. This work was performed under the Cooperative Research Program of "Network Joint Research Center for Materials and Devices. This work was performed under the Research Program of "Dynamic Alliance for Open Innovation Bridging Human, Environment and Materials" in "Network Joint Research Center for Materials and Devices". The authors thank Masayuki Kishino (Tokyo Tech), Kohsuke Matsumoto (Tokyo Tech), Kayoko Tokumitsu (Tokyo Tech), Yurina Kanehara (Tokyo Tech) and Accoc. Prof. Shoichi Kubo (Tokyo Tech) for fruitful discussions.

References

1 F. Garnier, G. Horowitz, X. Peng and D. Fichou, *Adv. Mater.*, 1990, **2**, 592.
2 G. Gustafsson, Y. Cao, G. M. Treacy, F. Klavetter, N. Colaneri and A. J. Heeger, *Nature*, 1992, **357**, 477.
3 F. Garnier, R. Hajlaoui, A. Yassar and P. Srivastava, *Science*, 1994, **265**, 1684.
4 P. K. Ho, Science, 1999, **285**, 233.
5 M. I. Nugraha, H. Matsui, S. Watanabe, T. Kubo, R. Häusermann, S. Z. Bisri, M. Sytnyk, W. Heiss, M. A. Loi and J. Takeya, *Adv. Electron. Mater.*, 2017, **3**, 1600360.

6 T. Kubo, R. Häusermann, J. Tsurumi, J. Soeda, Y. Okada, Y. Yamashita, N. Akamatsu, A. Shishido, C. Mitsui, T. Okamoto, S. Yanagisawa, H. Matsui and J. Takeya, *Nat. Commun.*, 2016, **7**, 1.
7 K. Fukuda, K. Yu and T. Someya, *Adv. Energy Mater.*, 2020, **10**, 2000765.
8 S. Kim, H.-J. Kwon, S. Lee, H. Shim, Y. Chun, W. Choi, J. Kwack, D. Han, M. Song, S. Kim, S. Mohammadi, I. Kee and S. Y. Lee, *Adv. Mater.*, 2011, **23**, 3511.
9 C. Wang, D. Hwang, Z. Yu, K. Takei, J. Park, T. Chen, B. Ma and A. Javey, *Nat. Mater*., 2013, **12**, 899.
10 S. Xu, Y. Zhang, J. Cho, J. Lee, X. Huang, L. Jia, J. A. Fan, Y. Su, J. Su, H. Zhang, H. Cheng, B. Lu, C. Yu, C. Chuang, T. Kim, T. Song, K. Shigeta, S. Kang, C. Dagdeviren, I. Petrov, P. V. Braun, Y. Huang, U. Paik and J. A. Rogers, *Nat. Commun*., 2013, **4**, 1543.
11 K. Takei, W. Honda, S. Harada, T. Arie and S. Akita, *Adv. Healthcare Mater.*, 2015, **4**, 487.
12 K. Xu, Y. Lu and K. Takei, *Adv. Mater. Technol.*, 2019, **4**, 1800628.
13 M. Xie, K. Hisano, M. Zhu, T. Toyoshi, M. Pan, S. Okada, O. Tsutsumi, S. Kawamura and C. Bowen, *Adv. Mater. Technol*., 2019, **4**, 1800626.
14 L. Zhang, S. Chizhik, Y. Wen and P. Naumov, *Adv. Funct. Mater.*, 2016, **26**, 1040.
15 A. Priimagi, C. J. Barrett and A. Shishido, *J. Mater. Chem. C*, 2014, **2**, 7155.
16 H. E. Fowler, B. R. Donovan, J. M. McCracken, F. López Jiménez and T. J. White, *Soft Matter*, 2020, **16**, 330.
17 H. Doi and K. Urayama, *Soft Matter*, 2017, **13**, 4341.
18 K. D. Harris, A. L. Elias and H.-J. Chung, *J. Mater. Sci.*, 2016, **51**, 2771.
19 L. Mao, Q. Meng, A. Ahmad and Z. Wei, *Adv. Energy Mater.*, 2017, **7**, 1700535.
20 L. Li, Z. Wu, S. Yuan and X.-B. Zhang, *Energy Environ. Sci*., 2014, **7**, 2101.
21 G. Zhou, F. Li and H.-M. Cheng, *Energy Environ. Sci*., 2014, **7**, 1307.
22 V. Zardetto, T. M. Brown, A. Reale and A. Di Carlo, *J. Polym. Sci. Part B Polym. Phys.*, 2011, **49**, 638.
23 T.-I. Lee, W. Jo, W. Kim, J.-H. Kim, K.-W. Paik and T.-S. Kim, *ACS Appl. Mater. Interfaces*, 2019, **11**, 13416.
24 S.-I. Park, J.-H. Ahn, X. Feng, S. Wang, Y. Huang and J. A. Rogers, *Adv. Funct. Mater.*, 2008, **18**, 2673.
25 J. Lewis, *Mater. Today*, 2006, **9**, 38.
26 M. T. Brannum, A. D. Auguste, B. R. Donovan, N. P. Godman, V. M. Matavulj, A. M. Steele, L. T. J. Korley, G. E. Wnek and T. J. White, *Macromolecules*, 2019, **52**, 8248.
27 J. P. Gong, *Soft Matter*, 2010, **6**, 2583.
28 J. Sawada, D. Aoki, H. Otsuka and T. Takata, *Angew. Chem. Int. Ed.*, 2019, **58**, 2765.
29 Y. Higuchi, *Polym. J.* **2018**, *50*, 579.
30 M. Kishino, N. Akamatsu, R. Taguchi, K. Hisano, O. Tsutsumi and A. Shishido, *J. Photopolym. Sci. Technol.* 2020, **33**, 81.
31 N.-J. Jo, A. Takahara and T. Kajiyama, *Polym. J.*, 1993, **25**, 721.
32 N. Kaiya, A. Takahara and T. Kajiyama, *Polym. J.*, 1989, **21**, 523.
33 T.-T. Mai, Y. Morishita and K. Urayama, *Soft Matter*, 2017, **13**, 1966.
34 N. Akamatsu, W. Tashiro, K. Saito, J. Mamiya, M. Kinoshita, T. Ikeda, J. Takeya, S. Fujikawa, A. Priimagi and A. Shishido, *Sci. Rep.*, 2014, **4**, 5377.
35 N. Akamatsu, M. Fukuhara, S. Fujikawa and A. Shishido, *J. Photopolym. Sci. Technol.*, 2018, **31**, 523.
36 N. Akamatsu, K. Hisano, R. Tatsumi, M. Aizawa, C. J. Barrett and A. Shishido, *Soft Matter*, 2017, **13**, 7486.
37 K. Kuwahara, R. Taguchi, M. Kishino, N. Akamatsu, K. Tokumitsu and A. Shishido, *Appl. Phys. Express*, 2020, **13**, 056502.
38 N. Ando, K. Hyodo, H. Sasaki, Y. Ota, N. Terasaki, T. Sasayama, Y. Yokoi, A. Shishido, N. Akamatsu and R. Taguchi, *SID Symp. Dig. Tech. Pap.*, 2020, **51**, 417.
39 R. Taguchi, N. Akamatsu, K. Kuwahara, K. Tokumitsu, Y. Kobayashi, M. Kishino, K. Yaegashi, J. Takeya and A. Shishido, *Adv. Mater. Interfaces*, 2021, **8**, 2001662.
40 S. P. Timoshenko and J. M. Gere, *Theory of Elastic Stability*, McGraw Hill, New York, 1961.
41 M. C. Boyce and E. M. Arruda, *Polym. Eng. Sci.*, 1990, **30**, 1288.